Technical Report

Human-Powered Vehicle

An Undergraduate Thesis

Presented to the Faculty of the School of Engineering and Applied Science

University of Virginia · Charlottesville Virginia

In Fulfillment of the Requirements for the Degree

Bachelor of Science in Engineering

Author

Christopher Wilks

April 18, 2020

ASME Report Cover Page & Vehicle Description Form

Human Powered Vehicle Challenge
Competition Location: Michigan State University
Competition Date: April 3 - 5, 2020

This required document for <u>all</u> teams is to be incorporated into your Design Report.

<u>Please Observe Your Due Dates</u>; see the ASME HPVC website and rules for due dates.

Vehicle Description

University name: **University of Virginia**
Vehicle name: **Blue Comet**
Vehicle number: **34**
Vehicle configuration:

Upright _____ Semi-recumbent __**X**__
Prone _____ Other (specify) _____

Frame material: **AISI 4130 steel**
Fairing material(s): **Plastic**
Number of wheels: **3**
Vehicle Dimensions (in)
- Length: **105.70**
- Width: **33.91**
- Height: **48.73**
- Wheelbase: **45.15**

Weight Distribution (lb)
- Front: **30.58**
- Rear: **29.42**

Total Weight (lb): **60**
Wheel Size (in)
- Front: **20.0**
- Rear: **27.5**

Frontal area (in^2): **1410.50**
Steering (Front or Rear): **Front**
Braking (Front, Rear, or Both): **Front**
Estimated Coefficient of Drag: **0.167**

Vehicle history (e.g., has it competed before? where? when?): **The vehicle has not competed before.**

Human Powered Vehicle Team at the University of Virginia

2020 ASME HPVC E-Fest North Design Report

Vehicle Name: Blue Comet

Vehicle Number: 34

Team Captains: Niphattha Wongwiset <nw9ca@virginia.edu>,
Kevin Meyers <km4fk@virginia.edu>
Faculty Advisor: Natasha Smith <nls5m@virginia.edu>

Team Members:

Sungwoo Cho
Samantha Davis
Matthew Evanko
Yongyi Jiang
Thomas Lee
Brian Lembo
Ian O'Donnell
Dana Poon
Geoff Shellady
Christopher Wilks

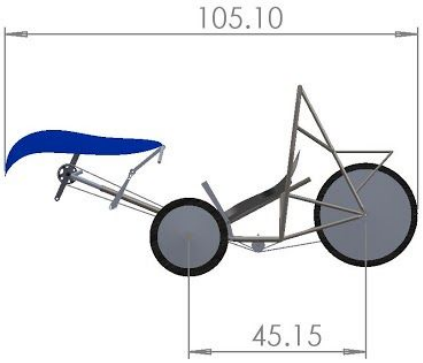

	NAME	DATE
DRAWN	K. MEYERS	2/13/20
CHECKED	N. WONGWISET	2/13/20
ALL DIMENSIONS IN INCHES		
WEIGHT:	60 LBS	

TITLE:
UNIVERSITY OF VIRGINIA
BLUE COMET
ASSEMBLY VIEW

DWG NO. 001

A4

SCALE:1:40

SHEET 1 OF 1

Abstract

The goal of the Human-Powered Vehicle team at the University of Virginia is to design and build *Blue Comet*, our human powered vehicle, to compete in the 2020 ASME HPVC E-Fest North. The team was established by 12 mechanical engineering undergraduate students with various engineering skills and experiences. Although this is the team's first time attending the competition, we have the passion and motivation to develop and apply our technical and interpersonal skills to completely build the bike. This design report lays out the conceptual development, background research, manufacturing process, modeling, computational analysis, and experimental testing used to build and optimize the vehicle's performance. The vehicle aims to obtain ride stability and high aerodynamic performance.

Blue Comet was designed as a three-wheeled, tadpole recumbent-trike constructed from AISI 4130 Steel. The boom provides the main structure for the vehicle with a symmetric axle and rear fork splits. An integrated Rollover Protection System (RPS) increases the rider's safety in the event of a crash. A removable transparent partial fairing is applied to increase the aerodynamic efficiency in the drag race while not compromising visibility. Since the members of our team have effective leg lengths ranging from 22 to 29 inches, we designed an extension rod for the crankset with seven inches of adjustability. The calculated average speed of *Blue Comet is 20* mph, according to gearing analysis of the design. With the high safety focus, the flexibility for riders, and the calculated high speed capabilities, we are confident that *Blue Comet* will be a successful, competitive vehicle in this year's HPVC North.

Table of Contents

1. Design

1.1 Design Objectives

The main objective of this project was to provide University of Virginia students the opportunity to apply the mechanical engineering principles being taught, such as the stress-strain relationship, power transfer through gears, and fatigue in design, by designing and building a physical product. Our design aims to use these principles to provide comfort, efficiency, and safety towards the manufacturing of a competitive human powered vehicle (HPV). The University of Virginia Blue team hopes that this will provide practical knowledge and experience that will translate to real design challenges in the engineering industry.

1.2 Background Research

Due to having little prior experience with HPV or bicycle construction, the team thoroughly researched each design component and garnered knowledge from the archive of HPVC reports. This section shows the research conducted during the design and building processes needed to optimize the performance of the vehicle. Specific components researched are: frame, fairing, steering, gearing and chain path, and ergonomics.

1.2.1 Frame

The frame is the backbone of a typical HPV and must provide structure and strength, as well as flexibility with regard to the constraints of the competition. The seat and wheel configurations were important considerations regarding the vehicle's structure, while material selection would affect both strength and weight.

The first major consideration for the frame was the seat configuration. Two that were considered were: conventional upright and recumbent configurations. Upright bicycles were found to have better stand up sprint capability than recumbents which leads to easier climbing [1], but recumbent bicycles experience more efficient energy expenditure and are more ergonomic [2]. Upright bicycles produce more strain on the upper body and back, whereas a recumbent causes more strain on the knees [3]. Additionally, upright bicycles are lighter weight and more agile than a recumbent. Efficiency was a higher design constraint and so the recumbent seating was chosen.

The second major consideration was the wheel configuration. Three different wheel configurations were considered: tadpole, delta, and two-wheeled. The tadpole has two wheels in the front, one in the back, and has a low center of gravity which promotes stability and this translates to better cornering at higher speeds [4]. The delta has one wheel in the front, two in the back, and possesses easier maneuverability than the tadpole, but has a tighter turning radius. The two-wheel configuration is lightweight due to its smaller frame and has less rolling resistance [5]. The tadpole configuration was chosen due to its greater stability which was the greater concern for the HPV.

The last major component was the material. Steel, aluminum, titanium, and carbon fiber are the most common materials used. Steel is commonly used because it is easy to bend and shape, it is affordable, easily repaired, while still offering excellent ride quality and durability [6]. Aluminum is the most popular frame material because it is light, strong, and stiff,

which gives riders a solid ride for climbing or lively handling in tight situations [6]. Titanium is considered one of the longest lasting and strongest frame materials and many cyclists believe it combines the best qualities of the other frame materials. However, titanium is also the most expensive material and is very hard on metalworking tools [6]. Carbon fiber is the most unique frame material because it is not a metal, it can be manipulated in various different ways, and it still provides light, stiff, and durable frames. However, carbon fiber is at the high end of the cost spectrum and tends to be brittle [6]. Due to time constraints and budget consideration, steel is the best option to build our frame.

Based on the background research of our options, it was determined that the recumbent seating provides the best efficiency and ergonomics, the tadpole wheel configuration adds better stability to the structure, and the steel frame will give it the strength we need while accommodating our budget and metalworking constraint. Therefore, our HPV will be a recumbent tadpole trike constructed from a steel frame which will give the best structure and strength given our time and budget constraints.

1.2.2 Fairing

The fairing on a typical HPV is meant to reduce the drag force acting on the vehicle. The most common ones found in human powered vehicles are partial or full fairings. With cost and manufacturability in mind, the team looked to previous HPVC teams for advice on how to construct the most effective fairing. Many vehicles had some variation of a fairing, whether it was a full or partial fairing. Full fairings were typically found to be more effective in reducing drag coefficients than partial fairings due to the increased coverage, and most of the top-performing vehicles had a full fairing. With regard to material, fiberglass, Kevlar, and carbon fiber were popular choices, with fiberglass being the more affordable option. Some designs featured a cloth or fabric fairing that was draped over the frames and sewn or taped to the frame [7], however, if improperly done, this could actually decrease the performance of the vehicle by essentially acting as a parachute. A partial or full fairing would be attached with screws or bolts to attachment bars that stem from the mainframe or roll cage. Further, quick-release fasteners can also be used for easier detachment than with permanent screws or bolts.

1.2.3 Steering

The primary considerations for the steering design lie in its geometry, specifically in the implementation of kingpin inclination and ackerman steering, as shown in Figure 1. Two other aspects to consider are the use of direct or indirect steering and the position of the handle bars.

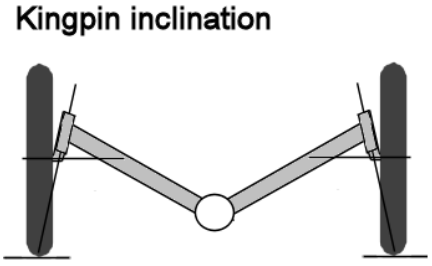

Figure 1*: 'Trike with zero scrub radius [8]*

The kingpin inclination is the angle of the hub's axis of rotation with respect to vertical. Kingpin inclination is used to control the scrub radius, which is the radius of the arc made by the tire's contact patch as it rotates about the axis of the knuckle. A lower scrub radius decreases the effort required to steer the vehicle, especially at low speeds [9]. Ackerman geometry is used to rotate the inside wheel more than the outside wheel when turning to account for the longer distance, and therefore larger turning radius, covered by the outside wheel. Adjusting the amount of ackerman compensation can alter the way in which energy is lost to friction during a turn [10].

The last two and secondary considerations for steering on recumbent bikes are whether to use direct or indirect steering, and whether the handlebars should be positioned underseat or overseat. For direct steering, the handlebars are connected directly to kingpins, which allows for simpler manufacturing and maneuverability [11]. In the indirect steering, the linkage is inserted between the handlebars and the kingpins to absorb vibrations along the ride. This absorption comes at the cost of having a more complicated manufacturing process and a higher weight [12]. In the position of the handle bars, underseat steering locates the handlebars along the side of the seat base [13] while overseat steering positions the handlebars upward and in front of the seat, similar to a standard two-wheeled bicycle. The overseat steering is more user-friendly and familiar to people used to riding bicycles, it adds extra weight and can restrict the vision for the recumbent trike [14]. Overseat steering can also increase the drag force on the bike by increasing the frontal area.

1.2.4 Gearing & Chainpath

The key components of the drivetrain of a typical HPV are the pedals, cranks, chainrings, cogs, and derailleurs. The crank converts the motion of the rider's legs into rotational motion to drive the rear wheel, the chainring connects the pedals to the cranks, and the derailleurs move the chain onto different cogs to adjust pedaling difficulty. In simple terms, the difference between smaller and larger gears is that smaller gears are more difficult to pedal, but can reach higher speeds and larger gears are easier to pedal, but are optimal at lower speeds [15].

When considering the range of gears, there is a tradeoff that has to be made between closely spaced gears and a wide range of gears. Closely spaced gears allow riders to fine tune their bicycle into a comfortable cruising range whereas a wide range of gears allows riders to jump to very high or very low settings for changes in incline, but may be difficult for riders to find a cruising range as the jumps between gears may feel too large. Gear efficiency relates to how far and fast a rider can go with the least amount of energy expenditure. Although it is often suggested that gears should be spaced evenly from highest to lowest, it is in fact better to have gears closer together in the higher range with bigger jumps toward the lower range. The gears in the higher range should be closer together due to the proportional relationship between the square of speed and air resistance; if the rider wants to go twice as fast, he or she now needs eight times as much power. The wider spacing for the lower gears accounts for the cadence dropping as the rider downshifts and the resulting slight loss of momentum in making a gear shift [16].

The main goal for the chainpath is to minimize chain losses. These losses come mainly from a dirty chain, quality of the manufacturing, chain tension, and cross-chaining [17]. Each of these contributes some amount of power loss to the system. For a dirty chain, the chain and gears should be thoroughly cleaned. For quality of manufacturing, different manufacturers make their chains to different specifications and have different tolerances. The better the specifications and the tighter the tolerances of the parts creates a smoother traveling chain and mitigates losses. Chain tension adds losses when the chain is too loose and swings along its path introducing sideways motions which dissipates energy. If the chain were to hit something, it would also add a large loss from the impact and discharge of energy. To mitigate against this, the chain needs to be properly tensioned so there is no extra slack in either the lowest gear or the highest gear. But there also cannot be too high a tension in the biggest gears as this can cause the chain to break. Cross-chaining is the last main contributor to power loss. It occurs when the chain is angled greater than 3 degrees across the gears and it can cause 3 or more watts of loss. Cross-chaining is most likely when the chain is on the closet gear to the bike in the front and on the farthest one in the bike and vice-versa. To reduce these losses, the angle of the chain, especially the powerside, must remain within the three degree range [18].

1.2.5 Ergonomics

Following the frame's decision to build a recumbent trike, an optimal seat position was researched. A hip angle of 125 degrees yields the greatest power output for a recumbent bicycle [19]. As stated in [3], the rider also finds it most comfortable to sit at a recumbent angle between 22 and 28 degrees. These angles would allow the feet to be over the hips and help the rider get the most power from pushing against the seat rather than the downward gravitational force provided on an upright bicycle [3]. These angles will provide maximum efficiency and comfort for our riders.

1.3 Prior Work

As a new team, we have no prior work to expand upon, outside of individual experiences with welding and involvement in other professional engineering teams in the school. The design for this vehicle was started from scratch for this year. The team will be making up for the lack of prior work with background research, specifically looking into designs entered in previous HPVCs by other universities and researching individual bicycle components.

1.4 Organizational Timeline

Figures 2 and 3 show a timeline of the Blue Comet project. The project began in September 2019 with research done on commercially available recumbent trikes along with previous HPVs entered in past competitions by other universities. An initial design was created using Solidworks and then tested using: finite element analysis (FEA), computational fluid dynamics (CFD), gearing analysis, and biomechanical testing. The FEA testing ensured that the design would meet the safety requirements designated by ASME. CFD testing was performed using Autodesk CFD which provided confirmation that the fairing improves the aerodynamics of the HPV. We utilised UVA's biomechanics lab to test each rider's optimal seat position and their power output which helped us narrow down who would be riding during the competition. With all the research and data gathered, we began prototyping in late October.

Before beginning assembly, we reached out to the UVA faculty member who oversees the Baja Racing Club. With his help, we were able to learn how to weld and use the necessary tools to assemble our HPV. Once assembled, the HPV was tested and small design improvements were made.

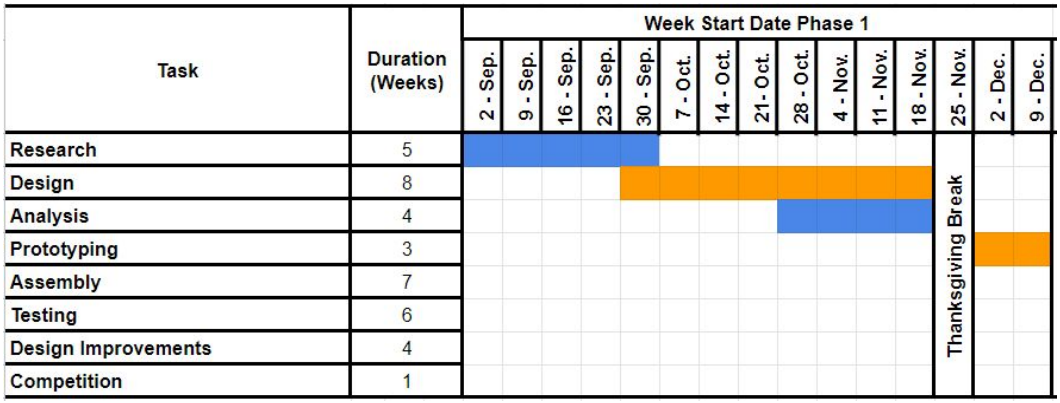

Figure 2: *Phase 1 of Timeline*

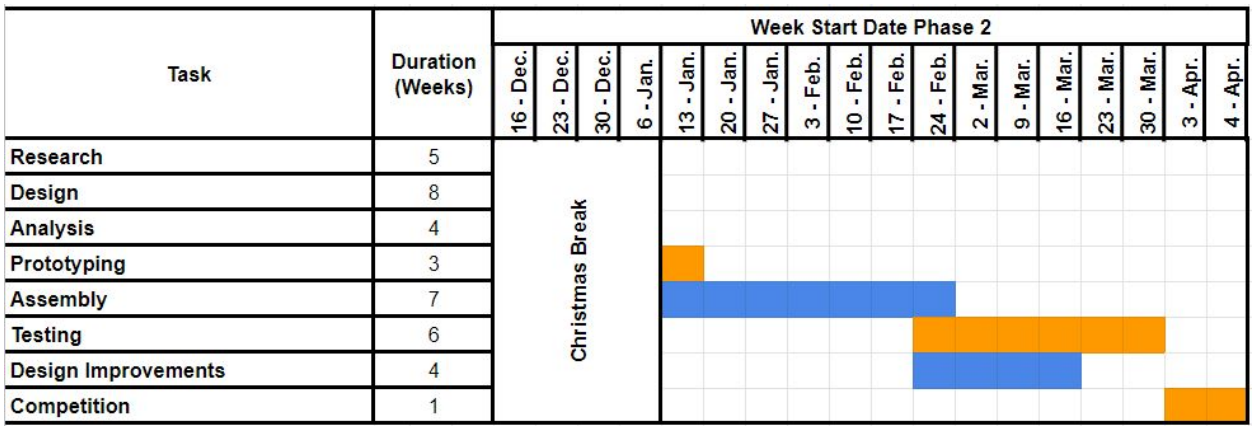

Figure 3: *Phase 2 of Timeline*

1.5 Product Design Specifications (PDS)

Table 1: *Product Design Specifications*

Requirement	Rationale
Comply with ASME rules and regulations	Ensure rider, participant, and spectator safety
Vehicle must be able to achieve a top speed of 35 mph with at least one male-identifying rider and one female-identifying rider	Reaching speeds of this magnitude is necessary to compete competitively in the speed event
Parcel storage for a 38x33x20 cm (max mass of 5.5 kg) reusable grocery bag	In order to maximize ease-of-use and maintain high performance, the vehicle must have a dedicated storage area

Vehicle must be able to accommodate riders with heights of 64 to 73 inches	Expected riders for this vehicle have heights that vary in this range
Finite Element Analysis must predict deformations less than 1 inch and indicate safety factors greater than 1.5 when loads are applied simulating riding conditions	These specifications ensure that the vehicle is durable and less prone to failure during the competition
180 degree field of vision for the rider	To ensure the vehicle's ease of use, maximize stability, and improve safety
Vehicle must be able to clear a 3.5 inches speed bump	The course may present bumps on the track that would compromise the vehicle's stability
Must be able to turn at an 8m radius	To ensure the vehicle will be able to take sharp turns on the course

1.6 Alternatives and Evaluation

As with any design process, the development of our vehicle went through several iterations. After deciding on the 3-wheel arrangement based on the background research, we had to determine our wheel layout as well as our frame material choice. As seen in section 1.7.1, a cross shaped frame was selected, as well as a tadpole wheel arrangement. These selections gave us an excellent foundation on which to base our initial vehicle design. Below is an initial and final frame rendering (Figure 4a and 4b).

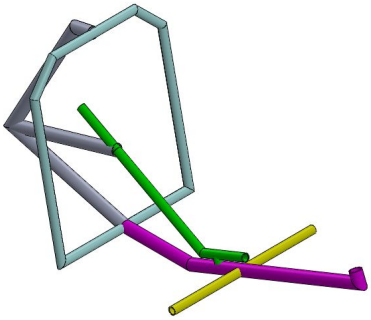

Figure 4a: *Initial frame design: rear fork (grey), seat support (green), main boom (pink), roll cage (light blue), and steering tube (yellow)*

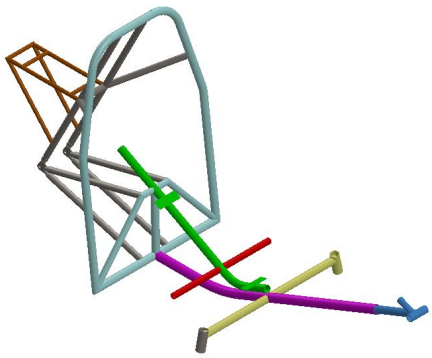

Figure 4b*: Isometric view of main frame: parcel rack (brown), rear forks (grey), seat support (green), main boom (pink), roll cage (light blue), handlebar connection tube (red), steering tube (yellow), and adjusting tube (blue)*

As can be seen in figure 4, some key differences came as the result of evaluating the frame at each stage of development. Notably, the sharp, welded corners of the initial frame gave way to a rounded RPS. This improved rigidity, and saved weight by requiring less material. Similarly, this preliminary design allowed for the seat to be adjustable to account for riders of varying heights. We used past expertise from our faculty advisor, Professor Smith, to decide that an adjustable crankset would prove superior to an adjustable seat because it would

maintain a rigid seat back and make the adjustment faster because the crankset can be adjusted to the right notch while the new rider is taking their seat. Another key change is in the rear wheel support section of the frame. The team had originally modeled a mono-fork in the rear. When forces and chainpathing for the rear wheel were evaluated we then modified this area to a traditional fork design. This not only improves rigidity, but allows for the vehicle to have a large parcel carrying area above the rear wheel.

While the current design has been through several iterations, it is possible that our finished vehicle will be different from the design seen above. Further testing will reveal which design alternatives prove successful, and which can be omitted from the final product.

1.7 Structured Design Methods

This section will focus on the design choices our team made over the course of this past year. The team made the design selection of each subsystem based upon background research and/or design matrices comparing the potential options to the traits considered.

1.7.1 Frame Design Selection

The team chose to use AISI 4130 steel, normalized at 870 °C, to build the frame. When compared to other accessible frame materials, 4130 was selected for its manufacturability and strength. The team evaluated three frame designs: Tub, Arrowhead, and Cross (Figure 5). A tub frame is a rectangular frame where two wheels are connected on the two front corners of the frame and another wheel is installed at the middle of the rear tube (Figure 5b). The arrowhead frame is a triangular-shaped frame where two wheels are installed at the two front corners of the triangle, and another one is installed at the rear corner (Figure 5c). Details of cross-frame are in section 2.1 Frame. The cross-frame was selected for the highest score received as shown in table 2.

Table 2*: Frame design selection matrix*

	Weighting	Tub	Cross	Arrowhead
Weight	40%		x	
Rigidity	35%	x		x
Protection	25%	x	x	
Total		60%	65%	35%

Figure 5a: Cross frame [20]

Figure 5b: Tub frame [21]

Figure 5c: Arrowhead frame[22]

1.7.2 Steering Design Selection

The design utilises direct steering with preference to its control at high speed and simplified manufacturing process [23]. The handle bars have extension rods and knuckles connected to the kingpins directly in order to turn the front wheels. To minimize weight, the underseat steering is preferable.

The brakes chosen for the design are cable-actuated disc brakes. Disc brakes are preferred for our purposes for a few reasons: their short stopping distance, their ability to hold up against heat from friction over long distances which will help prevent blowout, their dependency in any weather condition, and the ease with which they can be removed for repairs. The brakes are attached to a rotor on the hub of the wheel, and cable-actuated rather than hydraulic in order to make repairs easier and minimize risk.

1.7.3 Ergonomics Design Selection

The ergonomics were included in the design to ensure that the vehicle was optimized for efficient power output. Initially, the leg lengths of each team member were recorded (figure 6a) to determine the best dimensions of the tricycle to accommodate a large difference in rider heights. They were compiled in a histogram (figure 6b) and from that it was determined that we could best accommodate the leg length range between 41 and 47 inches to design our bike around. The resulting frame dimensions were created based off of these initial measurements for how adjustable the frame would need to be.

Additional background research was conducted to determine the ideal recumbency angle. The back angle was set at 28 degrees. This angle was later tested and confirmed for comfort using the Biodex machine shown in figure 6c. Next, the hip angle was set to 125 degrees. The connected body angles became dependent on this angle consistency. Based off of the background research conducted, this angle would provide the maximum power output provided by a rider in the recumbent position. After consulting with the frame designers, it was realized the dimensions of the bike did not agree with the hip angle provided. When the frame designers had modeled a human to ride our HPV, the frame dimensions and adjustable crankshaft caused the rider's hip angle to become very small. This resulted in the rider becoming very cramped in the seat, making it very uncomfortable for them. A change was

made to make the 101.5 degree knee angle [19] the dominant angle to ensure the overall comfort of the rider, thereby opening up the hip angles. The overall frame design was a collaboration between biomechanics, frame research, and testing.

Figure 6a*: Leg Length measurements being taken.*

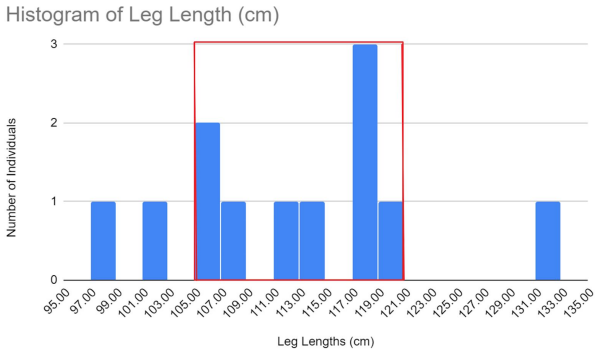

Figure 6b: *Histogram of all leg lengths and data collected from all team members and the selected range.*

Figure 6c: *Biodex testing biomechanics angles and taking data.*

1.7.4 Drivetrain Design Selection

The first decision in finding a gearing groupset was to choose between the overall set up of the gears, whether there would be shifting among both the chainring and the cassette (ex: 2x8, 3x8) or just the cassette (ex: 1x12). In Table 3, Gear Ratio Spacing refers to the gear ratio difference between one change in gears in the cassette, Gear Ratio Range refers to the gear ratio range between the highest and lowest possible gear ratios, and Fast Shifting refers to the ability to move across a large gear ratio range quickly.

Table 3: *Decision Matrix for Gearing*

	Weighting	3x7/3x8/3x10	2x7/2x8/2x10	1x12
Lightweight	20%			X
Simplicity	25%			X
Gear Ratio Spacing	5%	X	X	
Gear Ratio Range	15%	X	X	X
Cheap	10%	X	X	
Fast Shifting	10%	X	X	
Reliability	15%			X
Total		40%	40%	75%

After comparing the relevant parameters of the different set ups, we determined a simple 1x12 system allowed for simplicity and reliability, while still maintaining a large gear ratio range.

The chain path was designed to optimize power output specifically by avoiding interference with the frame, minimizing friction, minimizing cross-chaining, and providing the right chain tension throughout the route. The chain was chosen for manufacturing quality and its compatibility with the drive chain set. An idler would be needed to route the chain around the complex geometry of the frame to ensure that it would not interfere with the frame or rider at any point. Multiple single cogs were considered to pull or push the chain around the frame, single idlers were looked at, but the final choice was the TerraCycle Over/Under Idler for its durability and its cog on the powerside which will optimize power transfer on the power side. Plastic tubing was also considered to route the chain around the complex geometry but was ruled out for the additional friction it would introduce to the chain path. With proper placement of the idler, the chain could be routed properly without the additional guidance.

1.7.5 Fairing Design Selection

The decision of the fairing was based upon the team budget and performance improvements. The initial decision was between a partial and a full fairing. Table 4 shows the traits that were prioritized which include weight, visibility, drag reduction, price, and accessibility. Setting a weighting on each trait depending on the level of importance, each fairing option was evaluated as shown in table 4.

Table 4: *Decision matrix for fairing type*

	Weighting	Full Faiiring	Partial Fairing
Weight	30%		x
Visibility	25%		x
Drag Reduction	15%	x	
Price	10%		x
Accessibility	20%		x
Total		15%	85%

As seen in Table 4, the partial fairing better fit our needs. Although a decision matrix was initially used to justify our decision on which fairing to use, we mainly decided to use a partial fairing due to the time and skill constraints related to making one from scratch. Our team decided that the time spent researching and making a fairing would be better spent improving other aspects of the bike. We believed that commercially available fairings would also be of higher quality than what we could manufacture.

2. Vehicle Description

2.1 Frame

The frame was designed to prioritize rider protection. The main boom used AISI 4130 steel tubing with a 1.5 inches outer diameter and 0.065 inches wall thickness. To save weight, the rear forks used 1 inch outer diameter tubing to provide sufficient structural support. The third type of tubing used in the trike was 1.25 inches outer diameter tubing with 0.065 inches thickness for the rollover protection system (RPS).

The design for the frame began by creating a spine with a tadpole layout. With a cross-shaped base to build from, an RPS was incorporated. A roll cage made of a single bent steel tube was added to maximize protection. An RPS made from a single bent tube is stronger than one made of multiple pieces welded together because it has fewer areas of stress concentration. To increase the structural integrity of the frame, supports were added connecting the back rest to the RPS. For the rear fork, which supports both the rear wheel and parcel shelf, two triangulated supports were incorporated and affixed to the RPS with reinforcing tubes. An overview of the frame design can be seen in Figure 7b.

Based off of the research done by the ergonomics team, the frame's angles were modified to prioritize specific angles of the knees and back to maximize the rider's power output and the comfort of the recumbent bicycle. The angles that were decided to incorporate in the final design are a 101.5 degree knee angle and a 28 degree back angle, as shown in Figure 7a. These angles provided the best comfort for the riders while making sure the angles aligned with the ergonomics research that had been done.

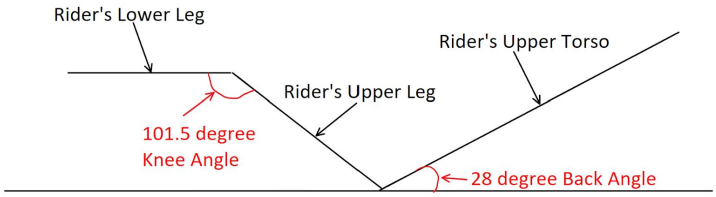

Figure 7a*: Diagram of angles required on our HPV*

The frame was optimized for the average rider of 68.5 inches. The weight of the final frame came out to be 26.61 lbs. Another key component of the frame design is the integrated pedal adjustment system. On the front of the boom is a tube perforated with holes. This allows for a similar, but smaller, diameter tube to fit inside and be attached with pass-through bolts. The tubing for the adjustable crank was manufactured using AISI 4130 Steel. The crankset on the end of this second adjustable member can then be operated by riders of heights varying from 63 to 73 inches, all while optimizing their seating position for the most power.

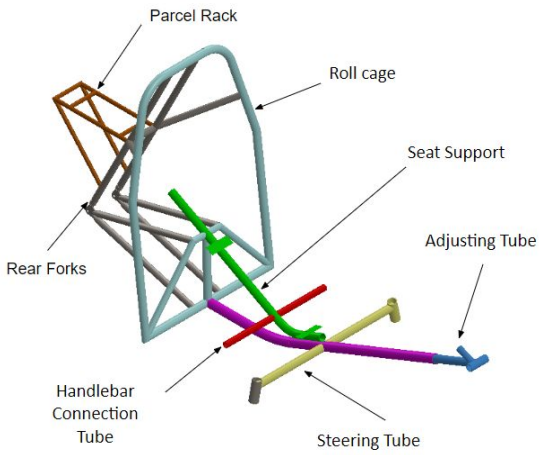

Figure 7b*: Isometric view of main frame: parcel rack (brown), rear forks (grey), seat support (green), main boom (pink), roll cage (light blue), handlebar connection tube (red), steering tube (yellow), and adjusting tube (blue)*

2.2 Steering

The steering system is designed to maximize durability and manufacturability, as well as allowing some level of adjustability to accommodate errors in the manufacturing process.

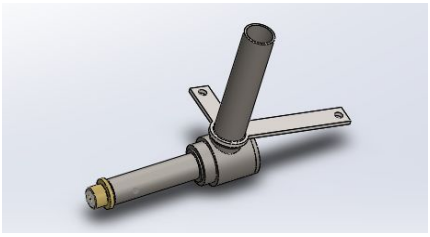

Figure 8a*:* Knuckle

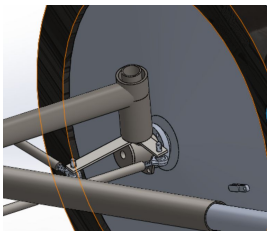

Figure 8b Axle Design and Frame Attachment

By using a knuckle design (Figure 8a) that closely mimics the interface of a bicycle fork's steerer tube with the head tube, we are able to make use of standard, off the shelf bicycle headsets to join the knuckles to the frame as shown in Figure 8b. Because the kingpin angle on the knuckle is less than the headtube angle on many mountain bikes, our use of these bearings falls within the scope of their intended application, minimizing the risk of failure. While the upright itself will be welded together, the axle will be attached via a press fit rather than welded to minimize warping that could occur when the part is heated during welding.

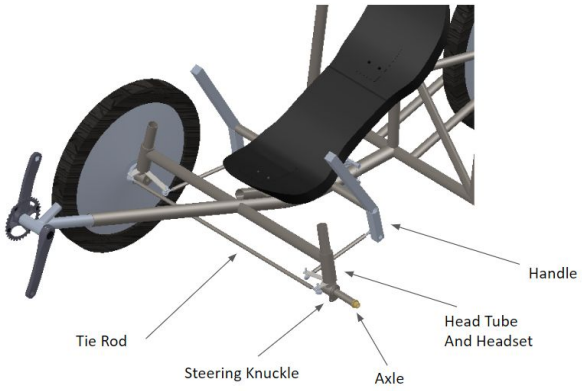

Figure 9*:* Full Steering Assembly

The two knuckles will be coupled using a tie rod positioned forward of the axes of rotation of the wheels (front steering). Due to the significant angle of the front portion of the frame, this positioning allows for increased clearance from the chain as well as the frame members. The rider will control the system using two handles positioned beside the seat which rotate to push and pull on drag links that connect to the wheels. Because both wheels could be controlled by an input from either handle, this system provides an element of redundancy in case of failure on one side. To allow for potential errors in alignment due to imperfect manufacturing of the frame tubes, the tie rod will be a turnbuckle-style connection that will allow for some amount of adjustment in length that is secured using jam nuts.

2.3 Gearing & Chainpath

The gearing set up is a 1x12 system, meaning that the crankset's chainring does not shift. The cassette, attached to the back wheel, is the only part shifting gears. The specific groupset this vehicle is equipped with is the SRAM NX Gearing Groupset, which includes a 12 ring cassette, crankset, shifter, bottom bracket, and chain (figure 10).

Figure 10: Components in the Groupset. a) cassette, b) crankset, c) shifter, d) bottom bracket, e) chain.

The chain path is routed between five components: The rear crankset, the front chainrings, the idler pulley, the rear derailleur (not shown), and the chain tensioner (not shown) (Figure 11). The chain path was designed to minimize losses and maximize power transfer by avoiding frame interference, minimizing cross-chaining, and providing the proper tension throughout the path. It will run from the front chainrings, through the chain tensioner, underneath the idler pulley on the power side, across the rear derailleur, to the rear crankset, back under the smooth side of the idler and return to the chainrings. The over/under idler pulley will be used to route both the top and the bottom of the chain under the front wheel mount and the steering tie-rod. It will also utilize a chain tensioner designed for recumbent tricycles to take up the slack from the adjustable pedals.

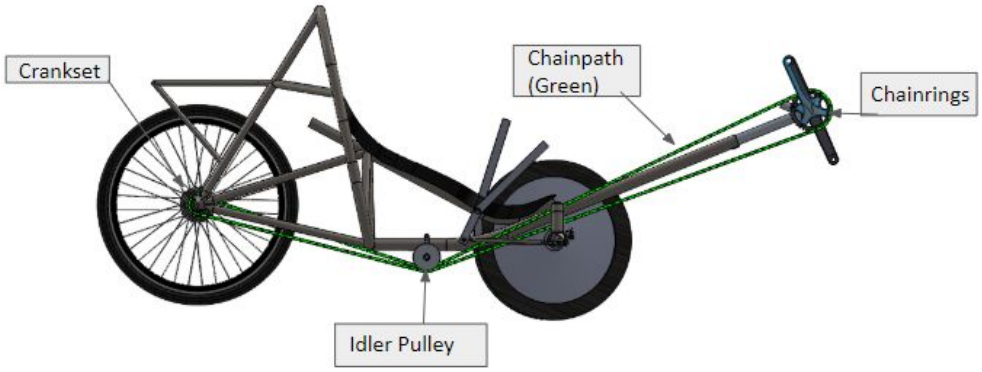

Figure 11*: The planned chianpath on the CAD model. Chain is highlighted in green. The rear derailleur and the chain tensioner are not shown.*

2.4 Fairing

The purchased fairing is manufactured by TerraCycle, a recumbent tricycle company. After researching their offerings, we decided on their WINTR fairing (Figure 10). This partial fairing is ideal because it is large and aerodynamic, yet transparent and fully adjustable for different riders. The mounting hardware clamps around the frame tubing (near the front derailleur post) and is attached to the fairing at 2 points for further adjustability. The WINTR fairing can be adjusted by simply moving it forwards or backwards (parallel to the ground). It can also be rotated, therefore adjusting the attack angle. The mechanism allows the fairing to open forward, giving the rider greater access for entry and exit. This angle-ability also allows the profile to be optimized for riders of different heights.

Figure 12: *TerraCycle WINTR Fairing*

3. Analysis

3.1 Rollover & Side Protection

According to Section III. D.1.a. and III. D.1.b. of the 2020 HPVC rules, an RPS design is acceptable if there is no indication of permanent deformation, fracture or delamination on either the roll bar or the vehicle frame, and the maximum elastic deformation is less than the specified amount for each load case. The finite element analysis (FEA) on the RPS was performed in Solidworks to validate the rider's safety in the rollover situation. The finite element model analyzed the frame structure using beam elements due to the thin shape of the tube profiles. To simulate the reaction force during the rollover situation, the harness attachment points are fixed in all RPS cases.

3.1.1 Top Load Modeling

The simulation model was prepared by removing non-structural parts in the frame to improve the time efficiency of the software. The model also combined the two bottom harness attachment points into one point since the beam supporting the seat which connects the rear part and main boom was simplified to a single beam. Because of the vehicle's adjustable leg extension, the simulation was tested in the "worst-case" scenario at the longest leg extension length at 44 inches using a single front boom by combining the main boom and the leg extension portion. The RPS top load case was simulated as described in the HPVC rules by applying 600 lbf distributed load on the top of the roll bar at an angle of 12 degrees from vertical using Solidworks Simulation 2019 with a static nodal stress analysis. Fixed constraints are applied at three harness attachment locations as shown in Figure 13.

3.1.2 Top Load Results

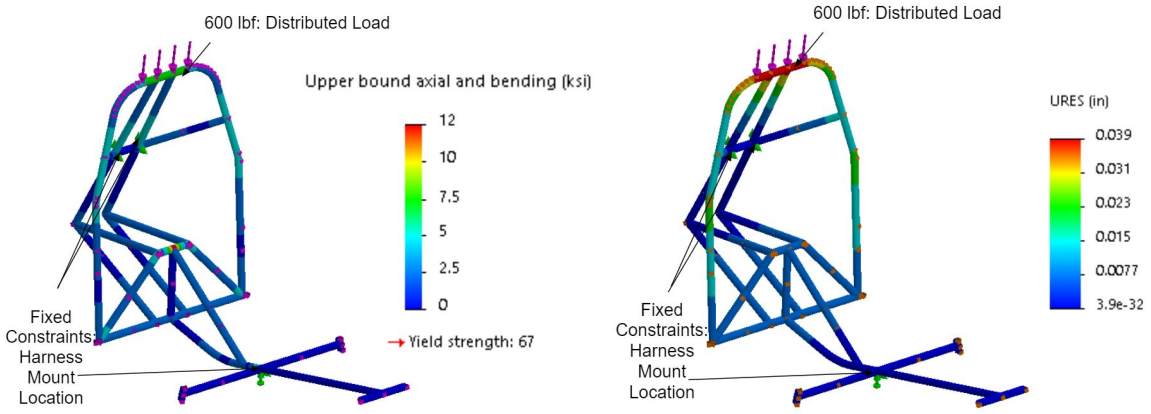

(a) *(b)*

Figure 13*: RPS top loading, constraints, stresses (a), and deflections (b)*

The maximum frame deflection from the top loading analysis, as shown in Figure 13, is 0.039 inches, which is well within the ASME requirement of 2 inches. The final FEA model consisted of a total of 1,279 nodes and 1,204 elements with a maximum von Mises stress of 12 ksi. Given the yield stress of 4130 steel, normalized at 870 °C, is 67 ksi, the factor of safety against yielding for the top loading case is 5.58.

3.1.3 Side Load Modeling

A similar model from the previous load case was applied to test on the side loading case by removing non-structural features, simplifying beams, and applying constraints at the harness attachment locations. The RPS side load case was simulated as described in the HPVC rules by applying 300 lbf distributed load on the side along the rider's shoulder as shown in Figure 14.

3.1.4 Side Load Results

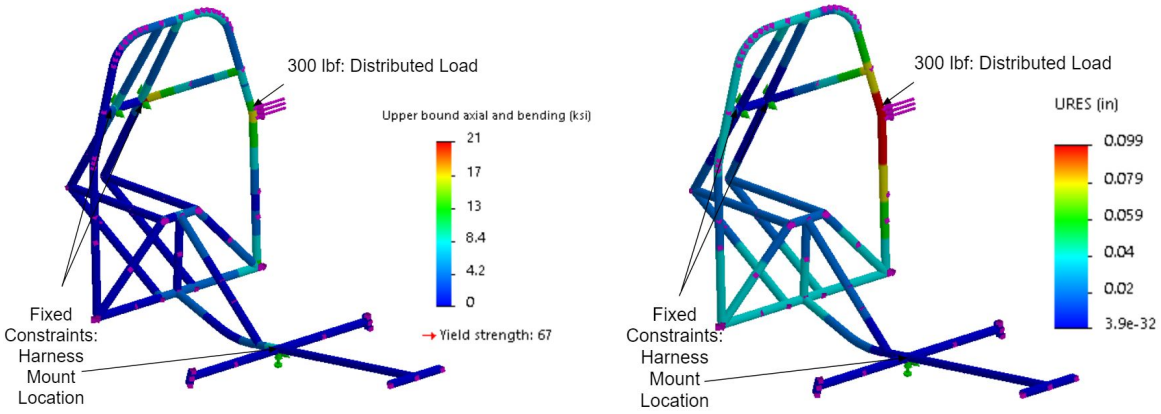

(a) *(b)*

Figure 14*: RPS side loading, constraints, stresses (a), and deflections (b)*

The maximum frame deflection from side loading analysis as shown in Figure 14 is 0.099 inches, well within the ASME requirement of 1.5 inches. The final FEA model consisted of a total of 1,279 nodes and 1,204 elements with 21 ksi maximum von Mises stress. Given the yield stress of 4130 steel, normalized at 870 °C, is 67 ksi, the factor of safety against yielding for the side loading case is 3.91.

3.2 Pedal Loading Analysis

3.2.1 Objectives

To ensure that a 1.5 inches outer diameter with a 0.065 inches wall thickness on the front boom is strong enough with a factor of safety higher than 1.50 and deflection lower than an inch when pedaling the bike.

3.2.2 Definitions

The resultant force from pedaling at the tip of the front boom was calculated from the forces acting on the free body diagram as shown in Figure 15. The maximum expected pedaling force, F_{pedal}, is 94.24 lbf, which was calculated using the maximum human pedaling power output from a pedaling biomechanics research article [19], the designed pedal radius, and an expected maximum pedalling speed of 80 rpm. Since the chain routing is parallel to the front boom at 22 degrees, the chain tension T_C was derived by summing moments about the center of the crankset. By solving from known forces, the resultant force was 298.98 lbf at 51.01 degrees from vertical.

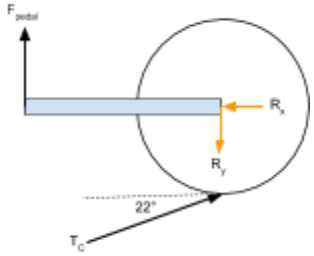

Figure 15: *Free body diagram of pedaling force, chain tension, and resultant force at front crankset*

3.2.3 Modeling

The previous model's constraints were adjusted to observe the deflection and stress of the vehicle by removing the harness attachment's constraints. In order to check the deflection at the front crankset, the seat mounting locations, front, and rear wheel connections are fixed. The 298.98 lbf load with 51.01 degrees from vertical was applied at the front crankset's location as shown in Figure 16.

3.2.4 Results

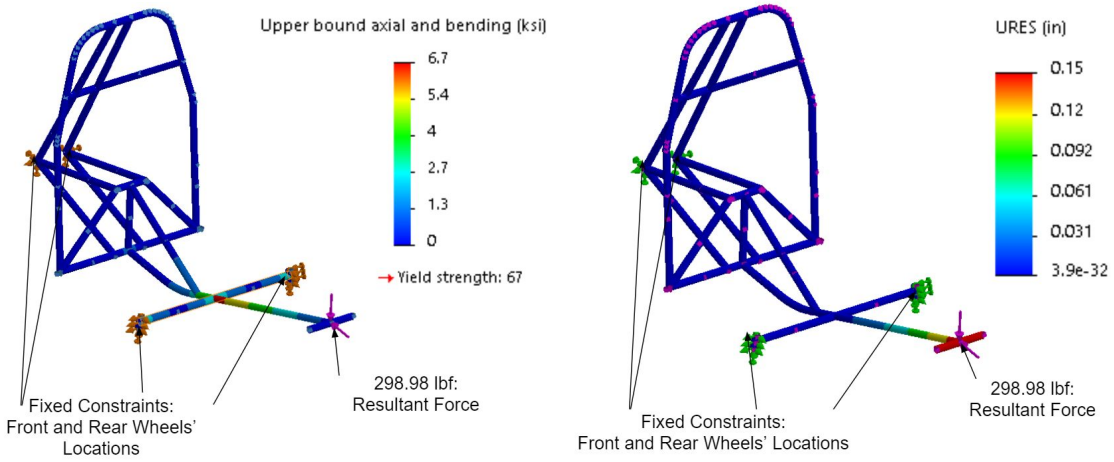

(a) *(b)*

Figure 16: *Pedaling loading case, constraints, stresses (a), and deflections (b)*

The maximum frame deflection from side loading analysis as shown in Figure 16 is 0.153 inches, well within the PDS requirement of 1.0 inches. Since the extension part has a smaller diameter, the additional mathematical calculation was applied, using deflection superposition method, as shown in appendix A. The corrected maximum deflection is 0.16 inches. The final FEA model consisted of a total of 1,279 nodes and 1,204 elements with 6.7 ksi maximum von Mises stress. Given the yield stress of 4130 steel, normalized at 870 °C, is 67 ksi, the factor of safety, against yielding, along on the top loading case is 10.

3.3 Back Loading Analysis

3.3.1 Objectives

To ensure that a 1.0 inches outer diameter with 0.049 inches wall thickness on the back support of the seat is strong enough with factor of safety higher than 1.50 and deflection lower than an inch during pedaling in service

3.3.2 Definitions

The back reaction force from pedaling was calculated by summing the moment about the center of mass of the rider as shown in the free body diagram in Figure 17. Since F_{pedal} is 94.24 lbf as shown in Figure 17, the back reaction force is 101.13 lbf at 28 degrees from vertical.

Figure 17*: Free body diagram of a rider with reaction forces during pedaling*

3.3.3 Modeling

Similar model from previous load case was applied to test on the pedaling load case in this study. In order to check the deflection and stress on the back support beam, the seat mounting locations front, and rear wheel connections are fixed. The 101.13 lbf load with 28 degrees from vertical was applied at the front crankset's location as shown in Figure 18.

3.3.4 Results

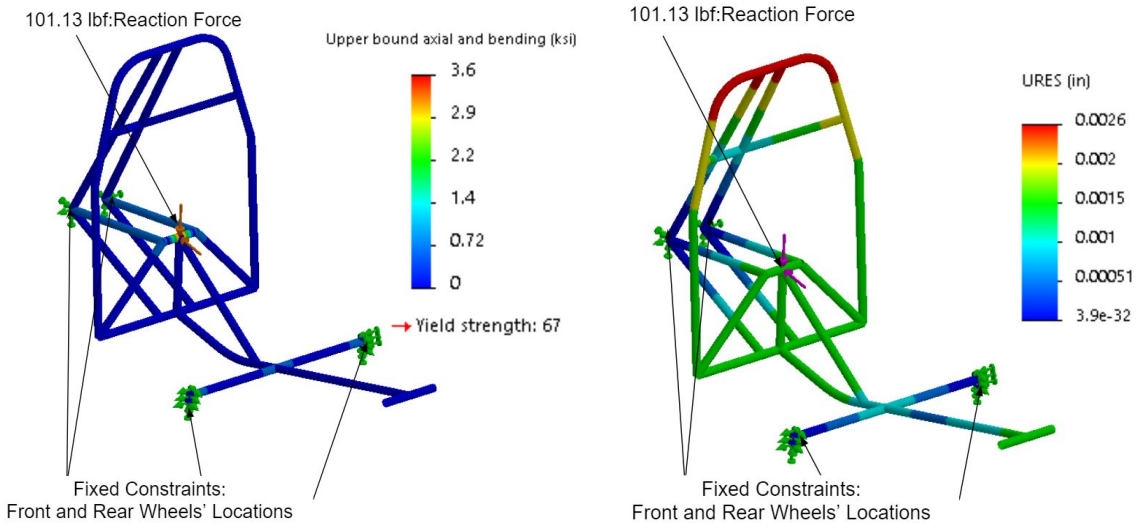

(a) *(b)*

Figure 18*: Reaction load on the back support beam during pedaling, constraints, stresses (a), and deflections (b)*

The maximum frame deflection from side loading analysis as shown in Figure 18 is 0.0026 inches, well within the PDS requirement of 1.0 inches. The final FEA model consisted of a total of 1,279 nodes and 1,204 elements with 3.6 ksi maximum von Mises stress. Given the yield stress of 4130 steel normalized at 870 °C is 67 ksi, the factor of safety, against yielding, along on the top loading case is 18.61.

3.4 Gearing Analysis

3.4.1 Objectives

Gears dictate the transfer of power from the rider to the bike to put themselves in motion. In order to get the most output of the vehicle, the gear ratios should be optimized. With the maximum speed goal of 35 mph, it was essential to use a chainring size that enables the vehicle to meet this condition. A larger chainring on the crankset can allow riders to cover more ground per pedal stroke, so 36 tooth chainring was chosen. In order to analyze a gearing set up and predict speed, the gear ratios are analyzed.

The gear ratio is only calculated from the first gear, which is the driving gear attached to the power source, and the last gear in the chain. In this case, it represents the amount of revolutions in the crankset per one revolution of the rear wheel. The higher the gear ratio means the pedal is more easily movable and vice versa. The gear ratios for a 36 teeth crankset, with cassette rings from 10 to 51 teeth are displayed below as this represents the set up of the vehicle.

3.4.2 Analysis

The following analysis pertains to gear ratios and the corresponding speed calculations that result from using a certain gear. In doing gear ratio calculations, the resulting metric is found by dividing the number of teeth in the cassette ring by the number of teeth in the driving gear (in this case, 36). To calculate the predicted speed of the vehicle, we assumed a gauge of the rider's stroke was maintained. Based on typical biking trends, the average rider can ride at a rate of 80 rpm and sprint close to the 120-140 rpm range for short bursts [24]. After making these assumptions and knowing the fastest speed will be achieved at the lowest gear ratio, 0.31 in this case, the speed is calculated by dividing the revolutions per minute by the lowest gear ratio and converting this into miles per hour with 27.5 inches rear wheel.

Table 6: Gear Ratios

10-51, 36T	
Driving Gear # of Teeth	
	36
# of Teeth	**Gear Ratio**
10	**0.28**
12	0.33
14	0.39
16	0.44
18	0.50
21	0.58
24	0.67
28	0.78
33	0.92
39	1.08
45	1.25
51	**1.42**

Table 7: Speed Calculations

	Low RPM	High RPM
RPM	80	120
Speed (MPH)	23.36	35.04
Torque (ft-lb)	17.6	2874
Power (hp)	0.268	4.31

Assumptions	
Weight of Rider (lb)	165
Weight of Bike (lb)	60
Frontal Area (ft^2)	6
Drag Coefficient	0.5
Drivetrain Loss (%)	15
Rolling Resistance	0.005
Density of Air (lb/ft^3)	0.07654

3.4.3 Results

The gear ratios span 0.28 to 1.42, which allows riders a wide range for tackling an uphill and looking to accelerate on a flat surface. Given the wheel sizes of the front and back wheels and the calculated lowest gear ratio (0.28), the predicted maximum speed of a rider sprinting at 120 rpm is 36 mph. However, considering the high power required to maintain this speed, it would be more realistic to expect an average speed of 20 mph.

3.5 Aerodynamic Analysis

In order to achieve the highest possible speed and do so efficiently while relying only on human power, the coefficient of drag must be as low as possible. In pursuit of this efficiency, a fairing would be a necessity in order to make the vehicle as aerodynamic as possible. To evaluate qualitative impacts of the fairing, we compared the drag coefficient between the base frame and the frame with a partial fairing using Autodesk CFD as shown in section 3.5.1. The model was placed in the volume box where the four side walls were set as slip/symmetry boundary conditions. The velocity of the wall facing the front of the vehicle was 20 mph while the back wall obtained a 0 psi static pressure. The enclosure material and vehicle material are air and solid respectively.

3.5.1 Chosen Design Substantiated

Once we decided on the Terracycle WINTR fairing, computational fluid dynamics analysis was used to prove the fairing's beneficial effects on the coefficient of drag. The analyses include two simplified trike models with a fairing and without a fairing as seen in the figure 19 and 20 to qualitatively compare the aerodynamic performance of the partial fairing.

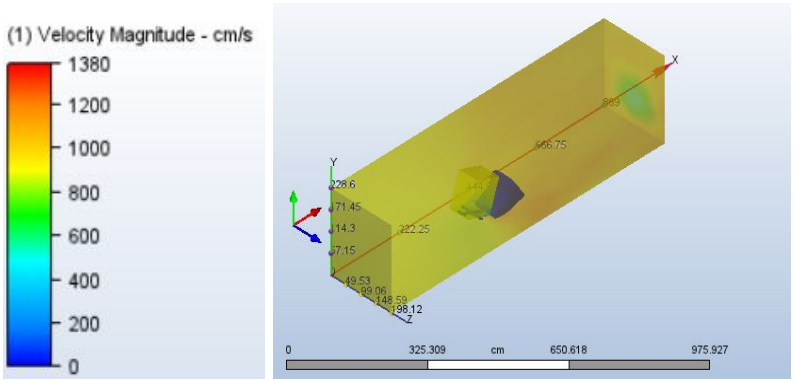

Figure 19: *CFD Analysis Without Fairing*

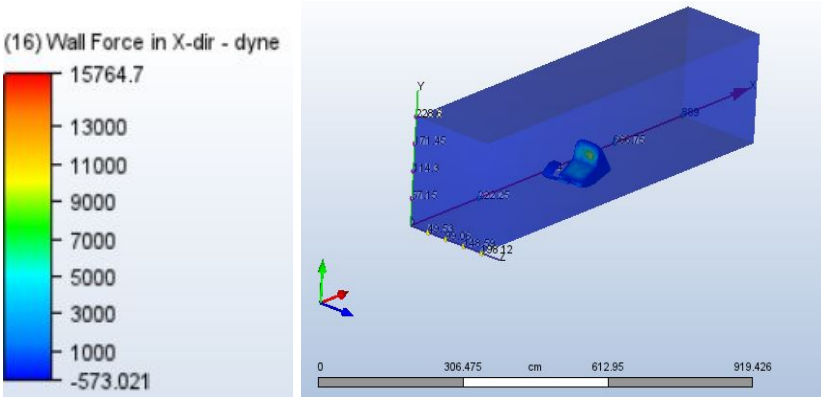

Figure 20: *CFD Analysis With Fairing*

The simulation includes the wall forces in the X, Y, and Z directions to further calculate the coefficient of drag, $C_D = \frac{2F_d}{\rho v^2 A}$, where air density (ρ) = 1.204 $\frac{kg}{m^2}$, area (A) = 4.529 m^2, and velocity (v) = 8.941 $\frac{m}{s}$. The respective total drag force and drag coefficient for two cases are shown in table 8.

Table 8: CFD Aerodynamic Result

Test Case	Drag Force (N)	Coefficient of Drag
Frame Base	40.32	0.185
Frame with a partial fairing	36.46	0.167

3.6 Cost Analysis

The original budget for our design team was $2000 from the department fund. However, after applying to multiple university grants, our current budget is now $6500 and we expect to receive more for transportation expenses. The team was also able to save a significant amount of money on parts by partnering with a local bike shop. The total vehicle's cost is $3,102.5. In table 9, the cost is categorized based on the main parts of the vehicle. The remaining budget was included in the expense during the competition including registration, transportation, and hotels for the team.

Table 9: *Blue Comet Bike Parts and Tooling Budget*

	Item	Cost
Frame	Steel Tubes	$505.16
	Fairing	$730.00
	Tooling kit/McMaster Carr	$430.00
	Parcel Basket	$20.00
	Welding filler material	$50.00
	Carrier basket	$15.00
	Total	$1,750.16

	Item	Cost
Miscellaneous/Safety	Harness	$50.00
	Lights	$25.00
	Rearview Mirror	$20.00
	Horn	$20.00
	Seat	$140.00
	Total	$255.00

	Total	$3,102.50

	Item	Cost
Drivetrain	Front wheel (20 in.) x 2	$220.90
	Idler pulley	$69.00
	Idler clamp	$43.00
	Boom tensioner	$155.00
	Rear tire	$9.79
	Cassette (12s, 11-50t)	$62.75
	Front tires (20 in.) x2	$27.98
	Rear wheel (27.5 in.)	$85.99
	Gear cables x3	$11.97
	Pedals	$8.69
	Disc brakes x2	$17.60
	Disc rotors x2	$35.98
	Chain connectors x4	$8.99
	Brake levers x2	$11.38
	Chains x2	$43.98
	Bottom bracket	$22.55
	Crankset	$68.65
	Derailleur	$66.65
	Trigger shifter	$26.55
	fees/tax	$99.94
	Total	$1,097.34

4. Testing

4.1 RPS Testing Plan

4.1.1 Objective & Methodology

The objective of the testing is to ensure the finished frame passes the safety requirement for riders under rollover scenario. Even though the computational test from FEA (section 3.1) proved that the frame will not overdeform from expected requirements, the experimental testing is necessary to ensure the frame can withstand under the criteria.

The methodology includes top loading and side loading scenarios. In the top loading case, the frame will be positioned 12 degrees from the vertical axis. The 600 lbf weight will be applied vertically at top of the roll cage, and the deflection will be measured accordingly. The frame will be flipped on the side loading case. The 300 lbf weight will apply vertically at the shoulder roll cage in the same position of the side loading case in section 3.1.4. Then, the deflection will be measured and recorded accordingly. The resulting deflections of top and side loading test cases are expected to be under 2 and 1.5 inches respectively. The results are also aimed to compare with those of the FEA models in order to further evaluate the setup of boundary conditions, as well as accuracy of computational and experimental testings.

4.2 Welding Testing plan

4.2.1 Objective & Methodology

The objective of welding testing is to ensure the welders are capable of making welds that are strong enough to withstand the forces to which the HPV will be subjected. The Instron Model 8874 was used for the tensile test. The specimens were constructed of three tubes with outer diameters of 1.25: two seven-inch tubes with a fish notch on one end and one six-inch tube. The two-seven inch tubes were welded inline with each other onto the six-inch tube, as shown in figure 21. The top and the bottom ends of the specimen were clamped into the tensile testing machine as shown in figure 22. The machine pulled the specimens until they fractured. The stress of fracturing was recorded for analysis.

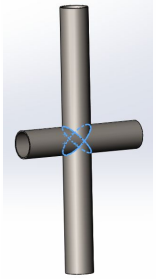

Figure 21*: Specimen of welding test. Highlighted edges are the welded edges.*

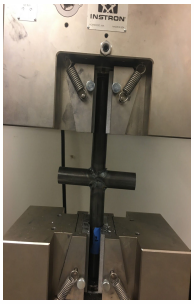

Figure 22: Tensile test setup

4.2.2 Results

Of the four specimens made, two of them were tested successfully. Of the other specimens, one was bent and could not be placed in the machine and the other slipped during the test and could not be put back into the machine.

The two specimens failed as follows: Specimen 1 failed when the top piece completely broke from the horizontal tube, and specimen 2 failed when both vertical tubes broke from the horizontal tube. In specimen 1, the weld on the lower tube remained intact. The upper piece failed mostly around the welded joint with one edge remaining connected to the tube and the stress caused the horizontal tube to split along the tubes welded joint, as can be seen in figure 23. The breakage location of specimen 2 was along our welded joint. The back edge of the upper vertical tube in figure 24 remained connected to the horizontal tube at the point of failure, and the other vertical tube tore off a piece of the horizontal tube (figure 24). The max forces and max stresses of the parts are recorded in table 10.

Figure 23 : *Testing specimen 1*

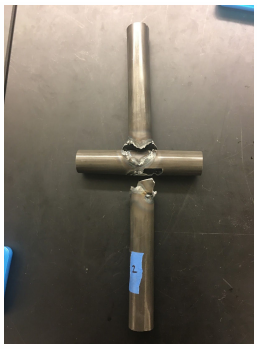

Figure 24: *Testing specimen 2*

4.2.3 Analysis

Given that the weld failed before the material, careful analysis of the stresses at which the weld failed are critical in determining if the weld is strong enough to withstand the forces the bike will undergo. As recorded in table 10, the max stress of specimen 1 is 220 ksi and the max stress of specimen 2 is 307 ksi. Comparing this to the maximum calculated stress of 21 ksi from the FEA for the RPS top and side loading, we can calculate safety factors of 10.4 for specimen one and 14.6 for specimen 2.

Table 10: *Breaking stresses of specimens. The safety factor is calculated using a maximum working load of 21 ksi.*

	Specimen1	**Specimen2**
Breaking Stress (ksi)	220	307
Breaking Force (kip)	13.7	19.2
Safety Factor	10.4	14.6

4.2.4 Conclusions

The welder is capable of making qualified welds on the HPV. With a minimum safety factor for the parts tested of 10.4 in tensile loading, the welds will be strong enough to withstand the forces on the HPV.

4.3 Chain Route Testing

4.3.1 Objective & Methodology

The main objective of chain route testing is to optimize power transfer by minimizing power losses. Additional objectives are to ensure the chain path will not hit against any portion of the frame and that it will not interfere with the rider as they pedal.

The first part of the test will be assembling all of the components on to the completed frame and testing for contact with any part of the frame. If there is any contact, the idler and boom tensioners will be adjusted to a position where they can route the chain around the frame pieces. Once there is no contact between the chain and the frame, testing will move on to identify losses' location and optimize against them. The process specifically starts with cross

chaining and then moves onto chain tension.

4.4 Biomechanics Testing

4.4.1 Objective & Methodology

It is understood that by utilizing human power as the source of propulsion, predicting power output and efficiency can be a complex task. Several steps have been taken to gauge rider performance capabilities. With the use of a Biodex System 3 muskuloskeletal performance measuring device, predicted riders had the opportunity to sit in a recumbent bike environment similar to that of the recumbent trike design (figure 25). With comfort in mind, riders were asked to find their preferred seat and pedal positioning so the angle could be recorded and incorporated into the design for the seat.

Once the HPV is completed, the team will be conducting muscle performance analysis while riding the actual vehicle using wearable electromyography (EMG) sensors. This will allow the leg muscle activation to be measured in the participating riders. Members of the team will wear the sensors while riding the bike around a track for a planned period of time. The EMG data on key leg muscle groups will be collected over time and analyzed for fatigue and optimal pedal positioning for maximized muscle activation. In addition, speed odometers will be utilized to assess stamina and performance over time.

4.4.2 Results and Discussion

Each person when setting positioning preferences found that the comfortable range of motion is very flexible. Different riders with different heights and leg lengths found they could sit at the same setting as one another quite comfortably.

The anticipated EMG and speed tests are to be utilized in order to assess the performance capabilities of the team's riders. Existing published techniques allow EMG data to be assessed for fatigue, which would help the team predict points at which riders would be subject to decreased performance and higher risk for injury. EMG data would also help fit the riders to their ideal seating positions, maximizing muscular potential. Speed data would be cross-examined with the EMG fatigue data.

Figure 25: *Biodex testing biomechanics angles and taking data.*

4.4.3 Conclusions

It was observed that there were not particularly obvious 'best positions' for each rider. It appears as though, within a reasonable range, distance to pedals and back angles can vary and still be comfortable. Through the utilization of wearable EMG sensors and collecting performance data such as speeds, we can assess the abilities of our riders and establish optimal

seat adjustment for each person. These tests will be conducted following the construction of the vehicle.

5. Conclusion

5.1 Comparison

Table 11 shows that the comparison of the analytical results meet or exceed the design specifications in stated in section 1.5.

***Table 11**: Comparison of Expected and Analytical Results for Design Specifications*

Design Specifications	**Expected Results**	**Analytical Results**
RPS top load case (600 lbf) deformation	< 2 in	0.039 in
RPS top load case (600 lbf) factor of safety, against yielding	> 1.5	5.58
RPS side load case (300 lbf) deformation	< 1.5 in	0.099 in
RPS side load case (300 lbf) factor of safety, against yielding	> 1.5	3.91
Parcel storage for reusable grocery bag	Weld the steel rack above the rear wheel	
Maximum vehicle speed	35 mph	35.04 mph
Vehicle must be able to accommodate riders with heights of 64 to 73 inches: extension rod provided length	7 in	7 in
Pedaling case: deformation	< 1 in	0.16
Pedaling case: factor of safety, against yielding	> 1.5	10.00
Back loading case: deformation	< 1 in	0.0026
Back loading case: factor of safety, against yielding	> 1.5	18.61

5.2 Evaluation

Blue Comet was evaluated primarily based on the design specifications. The computational tests, FEA and CFD, and experimental tests were applied to ensure that the design meets expectations. During the design phase, weekly meetings and updates helped limit the unexpected issues or conflicts between parts in the vehicle. Some adjustments continue to be made in the manufacturing process, as more experience is gained.

5.3 Recommendations

The team identified specific issues for timeline planning and frame materials. Even though the process was on-time and agreed well as a team, the team hopes to have early manufacturing time prior to submitting the report. The team recommends emphasising early welding and notching practice, allowing training to inform design decisions. Given the difficulty of welding curved pieces, especially for inexperienced welders, early and consistent practice

should be part of the team schedule and should be alleviated when possible in the design process. Since the construction phase started after winter break, the report lacks evaluation for the physical vehicle. In order to improve riders' performance, lighter total weight is meaningful. Therefore, aluminum should be considered for future vehicles.

References

[1] “The Advantages and Disadvantages of a Recumbent Bike.” California Spa and Fitness. https://thelookgoodfeelgoodstore.ca/blog/advantages-disadvantages-recumbent-bike/ (accessed Oct. 15, 2019)

[2] Mike. “Riding recumbent bicycles.” We Make Cycling Easy. https://www.wemakecyclingeasy.com/2016/12/03/riding/ (accessed Oct. 10, 2019).

[3] T. Dray. “The Best Leg Position for Recumbent Bicycles.” Live Strong. https://www.livestrong.com/article/556204-leg-position-recumbent-bicycles/ (accessed Oct. 15, 2019).

[4] “Recumbent Trikes.” Rad Innovations. https://www.rad-innovations.com/recumbent-trikes.html (accessed Oct. 10, 2019).

[5] J. Andersen. “Recumbent Bikes.” Bicycling Life. http://www.bicyclinglife.com/PracticalCycling/FancyBikes.htm (accessed Oct. 15, 2019).

[6] “Road Bike Materials.” City Bikes. https://www.citybikes.com/articles/road-bike-materials-pg57.htm (accessed Nov. 1, 2019).

[7] Clemson University (2017). *ASME.* Available: https://www.dropbox.com/s/s3nhxgsa62lnnbv/2017-hpvc-east-innovation-02-Clemson%20University.pdf?dl=0 (accessed Feb. 1, 2020).

[8] W. Beauchamp. “The Recumbent Racing Trike Page.” Recumbents. http://www.recumbents.com/wisil/trike/ (accessed Oct 20, 2019).

[9] B. Heißing and M. Ersoy, Eds., *Chassis Handbook: Fundamentals, Driving Dynamics, Components, Mechatronics, Perspectives*. Vieweg+Teubner Verlag, 2011.

[10] College of Engineering, “Ackerman? Anti-Ackerman? Or Parallel Steering?” The University of Alabama.

[11] M. Five, “Multi-Wheeled Vehicles,” Chunk Technical Documentation. http://dclxvi.org/chunk/tech/trike/index.html. (accessed Oct. 12, 2019).

[12] Mark, “Direct vs Indirect Steering,” Direct vs Indirect Steering, 27-Nov-2017. https://bentupcyclingjournal.blogspot.com/2017/11/direct-vs-indirect-steering.html. (accessed Oct. 12, 2019).

[13] “USS Recumbent Bicycles,” *Bicycle and Bikes*. https://www.bicycle-and-bikes.com/bicycle-buying-guide/recumbent-bicycles/uss-recumbent-bicycles/. (accessed Oct. 12, 2019).

[14] “OSS Recumbent Bicycles,” *Bicycle and Bikes*. [Online]. https://www.bicycle-and-bikes.com/bicycle-buying-guide/recumbent-bicycles/oss-recumbent-bicycles/. (accessed Oct. 12, 2019).

[15] S. Brown. “Gear Theory for Bicyclists.” Sheldon Brown. https://www.sheldonbrown.com/gear-theory.html (accessed Jan. 30, 2020).

[16] R. Howard. “True Ten Speed Drivetrains.” Bike Skills. http://www.bikeskills.com/more-choices-in-2011-1x10-2x10-or-3x10-drivetrains/ (accessed Jan. 30, 2020)

[17] J. B. Spicer, C. J. K. Richardson, Ehrlich et. al, "Effects of Frictional Loss on Bicycle Chain Drive Efficiency ." ASME. *J. Mech. Des*. 123(4), 598–605, Dec 2001, doi: 10.1115/1.1412848

[18] A. Guy. “TerraCycle Idlers and Your Trike’s Chainline.” Utah Trikes. https://www.utahtrikes.com/ARTICLE-37.html (accessed Nov. 12, 2019)

[19] J. W. Rankin, R. R. Neptune, “The influence of seat configuration on maximal average crank power during pedaling: a simulation study.” *Journal of Applied Biomechanics*, *26*(4), 493-500, Nov. 2010, doi: 10.1123/jab.26.4.493 (accessed Nov. 19, 2019).
[20] A. Prater (N.A) *Pinterest*. https://www.pinterest.com/pin/88664686391145489/ (accessed).
[21] T. Carabine. “The Carabine 741 Trike/DT Replica Project.” Virtualindian. http://www.virtualindian.org/trike.html (accessed).
[22] “Arrow-G3-Front.” Lancaster Recumbent. https://lancasterrecumbent.com/cycles/product/infento-childs-master-kit-for-building-bikes-trikes-and-scooters/arrow-g3-front/ (accessed Feb. 1, 2020).
[23] “Steering Design.” IHPVA. http://www.ihpva.org/Projects/tstrike/steering.htm (accessed Feb. 10, 2020)
[24] N.A (2017) “Different Types of Welding Joints.” *TOM*. *https://www.theweldingmaster.com/types-welding-joints/* (accessed Nov. 10, 2019).
[25] West Virginia University (2019). *ASME.* Available: https://drive.google.com/file/d/1T1MD1bm1UbTHepjgKnPIIWnJQNUB31jg/view (accessed Feb. 1, 2020)
[26] S. F. Brennan, A. G. Cresswell, D. J. Farris, and G. A. Lichtwark, “The Effect of Cadence on the Mechanics and Energetics of Constant Power Cycling,” *Med. Sci. Sports Exerc.*, vol. 51, no. 5, pp. 941–950, May 2019, doi: 10.1249/MSS.0000000000001863.

Appendix A : Mathematical Analysis for Pedaling Case

The deflection at 10 inches from the end-tip is where the transition between the main frame and transition rod occurs as shown in Figure 1A.

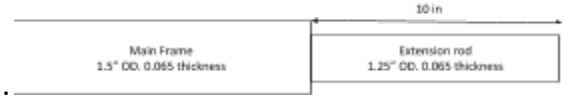

Figure 1A*: Extension rod and main frame geometry*

Then, the corrected mathematical calculation was applied from the transition to the end-tip using superposition approach as shown in Figure 1B, with 0.875 in the FEA deflection on the transition position.

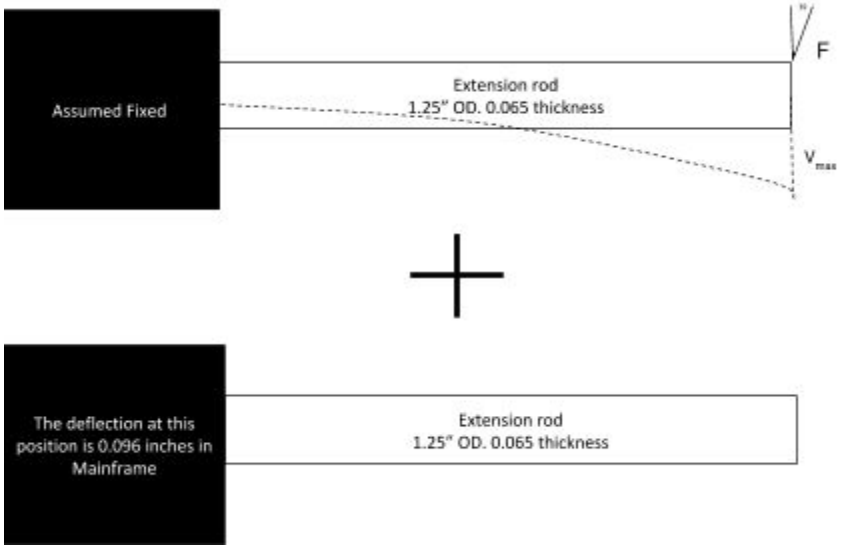

Figure 1B*: Superposition approach for corrected deflection*

**note: The angle of pedaling is 51 degrees from absolute vertical axis and 39 degrees with respect to the boom of the main frame neutral axis*

The corrected calculation part:

$v_{max} = -\frac{PL^3}{3EI}$,

where P is applied force perpendicular to beam = 298.98cos(39 **degrees)**

L is length of beam = 10 in

E is Young' modulus = 29.7 Mpsi

I is moment of inertia = $\frac{\pi}{64}(d_o^4 - d_i^4)$ = 0.043 inches

Therefore, the maximum deflection is 0.096 (from end of main frame's boom) + 0.064 (from extension rod part) = **0.16inches**